Arab J. Nucl. Sci. Appl., Vol. 51, 3, 22-31 (2018)

Arab Journal of Nuclear Sciences and Applications

ISSN 1110-0451 ***Web site: ajnsa.journals.ekb.eg*** **(ESNSA)**

Strong correlations between Structural and Magnetic Properties of Zn and Zr Substituted $CuFe_2O_4$ for Magnetic Temperature Controller applications

O. M. Hemeda [1], A. Tawfik [1], A. M. A. Henaish*[1] and B. I. Salem [1]

(1). Physics Department, Faculty of Science, Tanta University, Egypt

Received 26th Oct. 2017
Accepted 1st March 2018

The effects of tetravalent and divalent substitution on the physical properties of Cu ferrites, prepared by a double sintering ceramic technique, have been investigated. It was found that substitution of Zn and Zr simultaneously enhanced sintering process and crystallization. The initial permeability drops sharply at certain temperature for stoichiometric composition, which makes Zn/Zr co-doped NiFe2O4 spinel ferrites a very promising candidate for magnetic switch, magnetic temperature transducer (MTT) and temperature sensitive controller devices. Thus, the change of Curie temperature could be simply controlled by controlling the contents of Zn and Zr within CuFe2O4. From magnetic hysteresis loop measurements, magnetic moment increases by Zn and Zr substitution.

Keywords: CuFe2O4, Stoichiometric composition, XRD, SEM, Magnetic properties

Introduction

The chemical composition, heat treatment and type of substituted ions strongly affect the intrinsic parameters of ferrites such as magnetization, initial permeability, Curie temperature, grain size and structural properties [1]. The hysteresis loop is influenced by defects that retard the magnetic domain wall motion within the grains [2]. $CuFe_2O_4$ compound is a cheap material and has important magnetic and electrical properties for various technological applications.

The effects of Zn and Zr additives on the structure and magnetic properties of $LiZnFe_2O_4$ were reported [3].

During last few decades, a new type of temperature sensitive element used for construction of devices for controlling temperature was reported [4-8]. The idea of using such an element is based on the sudden change of initial permeability near Curie point [4]. The sensitivity and performance of the device using such magnetic temperature transducers (MTT) are a direct function of this sudden change. Its value is given by the slope of permeability versus temperature around Curie point.

The aim of this paper is to investigate the influence of Zn and Zr on structure, microstructure and consequently magnetic properties of $CuFe_2O_4$. A special attention was given to the slope of μ (T) curve, for applications such as magnetic temperature transducer and temperature controlling devices. The results are presented and discussed.

Experimental

Samples preparation

The composition $Cu_{1-x}Zn_{x+y}Zr_yFe_{2-2y}O_4$ series (with x = 0.1, 0.2, 0.3, 0.4, 0.5 and 0.6 and y = 0.00, 0.02, 0.04, 0.06, 0.08 and 0.10) were synthesized using a conventional double sintering ceramic method. CuO, ZnO, ZrO and Fe_2O_3 in molar ratio were used as stating precursors. The mixtures, in molar ratio, were grinded using an agate mortar for 7 hours, pre-sintered at 900°C for 4 hours under

Corresponding author: ahmed.henaish@science.tanta.edu.eg
DOI: 10.21608/ajnsa.2018.1933.1005

atmospheric conditions then left to cool gradually to room temperature. The obtained powders were pressed at room temperature under a pressure of 10 Ton/cm^2 (10^7 Pa) in stainless steel mould into two different shapes: (i) tablets with 2 cm of diameter and 0.4 cm thickness and (ii) toroid having 3 cm of external diameter, 2 cm of internal diameter and 0.5 cm height. Finally, the obtained pellets were sintered at 1100°C for 3 hours. The furnace was left to cool gradually by 2.5 C° /min to room temperature.

Characterizations

The as-prepared samples were checked by X-ray diffraction using a Philips model (PW-1729) diffractometer equipped with Kα-Cu radiation (λ = 1.5418 Å). A morphological study and chemical composition study were conducted using Scanning Electron Microscope model (J S M-5200 LV) with Electron Dispersive Spectrometer (EDS) attachment. The magnetic permeability (μ_i) for all toroid samples was measured as a function of temperature at a constant frequency f = 1 KHz using the universal BM591 bridge with three terminals network. The temperature around the sample is measured by Ni-Cr-Ni thermocouple. The measurements were carried from room temperature up to 825 K. The magnetization measurements were carried out at room temperature using vibrating sample magnetometer (VSM) Oxford OX8JTL, England, equipped with a magnet of 1 Tesla.

Results and Discussion

X-ray diffraction analysis

X-ray diffraction patterns for stoichiometric $Cu_{1-x}Zn_{x+y}Zr_yFe_{2-2y}O_4$ system are shown in Figure (1). For simplicity, stoichiometric ferrite system is assigned by (s). All the diffraction peaks were indexed which is referred to a single spinel cubic phase with a face centered cubic (fcc) structure. No additional diffraction peaks, which can be attributed to some impurities, are observed. The peaks located at 2θ = 29.7°, 35.0°, 42.7°, 53.2°, 56.2°, 62.2° and 73.5° can be assigned to (220), (311), (222), (400), (422), (511), (440) and (533) planes, respectively. Meanwhile, the relative intensity of the diffraction peaks increases with increasing Zn and Zr contents, indicating the enhancement of crystallization during sintering process by the addition of Zn.

Figure (2) shows the variation of the lattice parameter a with Zr and Zn contents. It can be noticed that with increasing Zn and Zr contents, the lattice parameter is nearly constant.

Crystallite size (t)

Figure (3) shows the effect of Zr and Zn contents on the evolution of the crystallite size (t). The crystalline size was estimated from XRD broadening of (311) peak using Scherer's formula [9]:

$$t = \frac{0.9\lambda}{B\cos\theta} \quad (1)$$

Where B is the full width at half maximum (FWHM) in radian.

It can be observed (see Figure 3) that the calculated crystallite size ranges from 65 - 90 nm.

Bulk density (D)

The theoretical density (Dx) of the spinel phase was calculated from the following equation [9]:

$$D_x = \frac{8M}{Na^3} \quad (2)$$

Where M is the molecular weight of the samples.

As shown in Figure (4), with increasing Zn and Zr contents, the theoretical density (D_x) decreases linearly, this has a larger value than the bulk density due to the presence of pores in the material. On the other hand, the bulk density (D) decreases with increasing Zn and Zr contents up to x = 0.2 and y = 0.02, then increases to reach a steady value for higher concentrations. It is reported that Zn addition enhances the grain growth due to the greater solubility in the solid state reaction at higher concentrations.

Figure (5) shows the relation between radius of tetrahedral (R_A) and octahedral (R_B) sites, respectively. The radius of tetrahedral site (R_A) increases with increasing Zr and Zn contents. In the case of octahedral site (R_B), the radius is constant till reaching the composition x = 0.2 and y = 0.02, followed by a decrease to reach a steady value for higher concentrations. The substitution of Zn^{2+} ions with radius 0.074 nm instead of Fe^{3+} ions with radius 0.064 nm at tetrahedral site leads to the increase of R_A. The substitution of Zn^{2+} ions at tetrahedral sites will enforce Fe^{+3} ions to migrate to octahedral sites and substitute for Cu^{+2} ions therefore leading to a decrease of R_B. The addition

of Zr^{2+} ions with a radius 0.079 nm does not affect the value of R_B due to the small ratio of Zr^{2+} ions.

Theoretical lattice parameter

The theoretical lattice parameter can be calculated using the values of R_A, R_B and R_0 from the following equation [10]:

$$a_{th} = \frac{8}{3\sqrt{3}}[(R_A + R_0) + \sqrt{3}(R_B + R_0)] \quad (3)$$

In order to calculate R_A and R_B, it is necessary to know the cation distribution which can be represented by the above equation. These cation distributions are given in Table (1) which can be estimated by a better matching between the theoretical and experimental lattice parameters. The expected cation distribution of the proposed systems may be given according to the following formulas:

For stoichiometric $(Zn_{x+y}Zr_{y-t}Fe_{1-x-2y+t})[Cu_{1-x}Zr_tFe_{1+x-t}]$,where t = 0.2y

As shown in Figure (6) the calculated lattice parameter (a_{th}) is constant along all compositions although, the value of (a_{th}) is always higher than (a_{exp}) which may be due to cations redistribution between octahedral and tetrahedral sites. For example, some Zr ions may occupy tetrahedral and octahedral site. Zr^{4+} ions first enter the A site for low concentration and then subdivided between A and B sites for high concentration [11]. About 95% of Cu ion occupy the B site whereas 5% only occupy the A site.

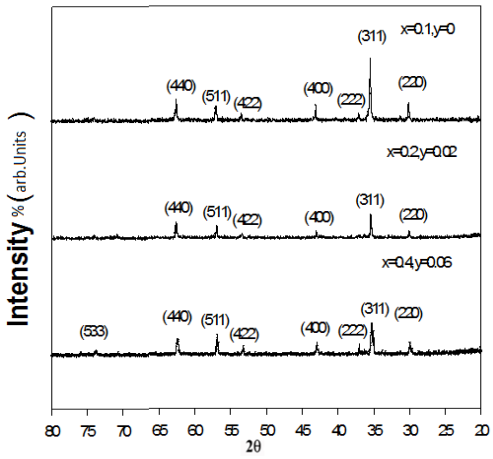

Fig. (1): The XRD pattern for (s) samples

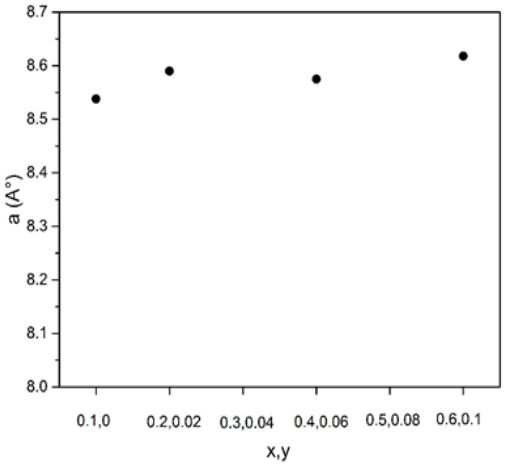

Fig. (2): The variation of lattice parameter a for (s) samples against x, y content

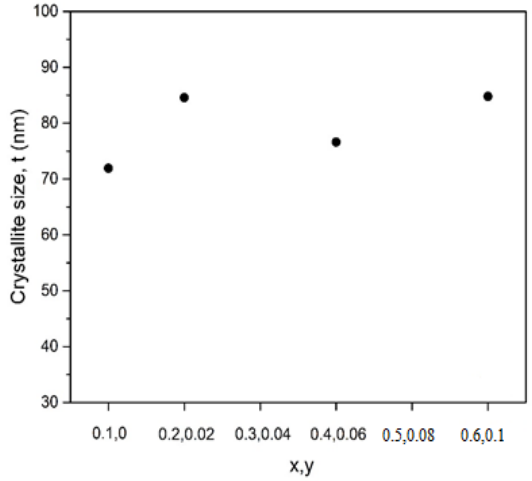

Fig. (3): Dependence of crystallite size t of (s) on x, y content

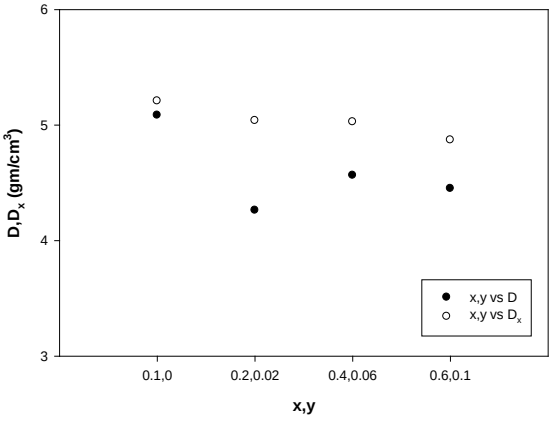

Fig. (4): Bulk (D) and theoretical (Dx) density for (s) samples.

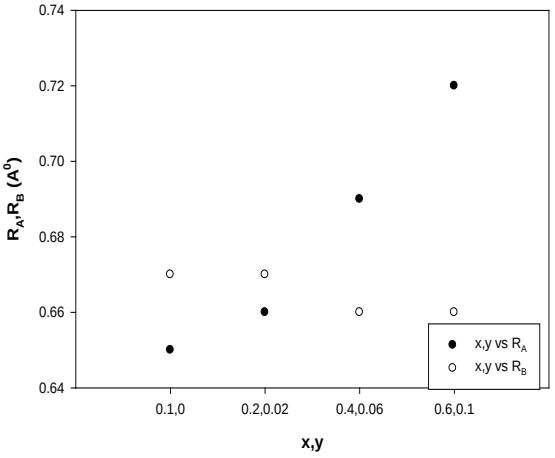

Fig. (5): R_A, R_B for (s) samples

Table (1): Cation distribution of (s) systems

Zr content	Zn content	Cation distribution
		Stoichiometric
y = 0.00	x = 0.1	$(Zn_{0.1}Fe_{0.9})[Cu_{0.9}Fe_{1.1}]$
y = 0.02	x = 0.2	$(Zn_{0.22}Zr_{0.016}Fe_{0.764})[Cu_{0.8}Zr_{0.004}Fe_{1.196}]$
y = 0.06	x = 0.4	$(Zn_{0.46}Zr_{0.048}Fe_{0.492})[Cu_{0.6}Zr_{0.012}Fe_{1.388}]$
y = 0.10	x = 0.6	$(Zn_{0.7}Zr_{0.08}Fe_{0.22})[Cu_{0.4}Zr_{0.02}Fe_{1.58}]$

Oxygen positional parameter

Considering that cations and anions have a spherical shape, A site is unable to accommodate available cation sites without local distortion. Hence A site expands towards the body diagonal of the cubic cell. A quantitative measure of this displacement is the oxygen positional parameter (u), its value for an ideal spinel ferrite structure is 0.375 Å. However, a slight deviation from the ideal value may occur due to relatively large radius of Zr ions which causes a distortion in the unit cell. The obtained results show that the value of oxygen positional parameter is greater than the ideal value and increases with increasing Zr content. The inversion parameter (δ), defined as δ = u - 0.375 for (s) system is the deviation from ideal u parameter which also increases with increasing Zr content. The values of oxygen positional parameter (u) and (δ) are given in Table (2), and calculated from the following relation:

$$(u) = \frac{r_{A+r_B}}{\sqrt{3}a} + \frac{1}{4} \qquad (4)$$

SEM analysis

Figure (7) shows SEM micrographs for $Cu_{1-x}Zn_{x+y}Zr_yFe_{2-2y}O_4$. Grains with different sizes were observed confirming the crystalline structure of the given ferrite phase which is in agreement with XRD results. The main process that affects the grain size is the enhancement of grain growth by the addition of Zn which accelerates the sintering process. Zn has a solubility limit in the solid state reaction. Another process that may occur during the sintering process is the retarding of grain growth due to Zr addition. Therefore, a competition between two processes occur during sintering of the studied ferrite systems due to the presence of both Zn (accelerates) and Zr (retards) grain growth mechanism. The value of the grain size is given in Table (3), which ranges from 14 to 70 µm.

The chemical composition of polycrystalline ferrite systems has been determined using Energy X-ray Analysis (EDS) as shown in figure 8. Quantitative analysis of EDS spectrum revealed the relative atomic ratio Fe: Cu: Zn: Zr which is close to the starting value of $Cu_{1-x}Zn_xZr_yFe_{2-y}O_4$ compositions. EDS analysis data are reported in Table (4).

Initial magnetic permeability

Compositional variation of initial permeability (μ_i) at 1 kHz as a function of temperature for various Zn and Zr contents is shown in Figure (9). It can be noticed that the permeability at room temperature increases with increasing x and y as shown in Figure (10). The increase in μ_i as Zr content increases can be attributed to the decrease in the magnetic anisotropy field by increasing temperature according to the following relation:

$$\mu_i = \frac{M_s^{\,2} D}{\sqrt{k}} \qquad (5)$$

Where K is the anisotropy constant, D is the grain size and M is the saturation magnetization [12].

The initial permeability sharply decreases at Curie temperature (T_c) which makes it a very

promising candidate for magnetic switches [13,14]. M_s drops suddenly almost to zero value at a temperature close to (T_c) , due to the ferri to para magnetic transition, leading to a rapid decrease of μ_i at T_c [15]. The value of T_c was found to decrease with increasing Zn and Zr contents. The substitution of diamagnetic Zn and Zr ions leads to a decrease in the A-B exchange interaction which reduces the magnetization and consequently Curie temperature decreases. From the above discussion, it is already shown that the presence of Zn and Zr ions in $CuFe_2O_4$ compound gives a rise to increase its initial permeability and an important decrease of Curie temperature. It was found that Curie temperature decrease from 708 to 488 K. It is therefore quite easy to obtain a magnetic material with a desired Curie temperature by simply controlling the contents of Zn and Zr within $CuFe_2O_4$.

The dependence of (μ_i) on temperature exhibits Hopkinson peak (HP) in the vicinity of Curie temperature (T_c) which confirms the phase purity of ferrite systems. The decrease of anisotropy field is faster than the decrease of the saturation magnetization with increasing temperature which leads to the presence of HP. Also, it can be seen that the sharpness of the peak decreases with increasing Zn and Zr contents, which may be associated with grain size variation.

The idea of using materials with optimized chemical composition and appropriate magnetic properties for the construction of controlling temperature devices is based on the sudden change of initial permeability near Curie temperature. Such materials are called magnetic temperature transducers (MTT). The sensitivity and performance of the devices using such materials are a direct function of the rate of change of permeability (slope). The higher the slope is the better the device for controlling temperature applications. The values of Curie temperature (T_c) and the rate of change of μ_i (slope of linear part) are given in Table (5).

Magnetic properties

Figure (11) shows the magnetic hysteresis loop of the studied systems. The as-prepared materials exhibit a typical magnetic hysteresis of a soft magnetic material, indicating that the materials are magnetically ordered. Substitution of Cu2+ and Fe3+ by Zn2+ and Zr4+ in (Cu1-xZnx+yZryFe2-2yO4) is expected to increase the value of the magnetic moment up to a certain limit, thereafter it decreases due to the canting of magnetic moment at B site. The dependence of saturation magnetization (Ms) on the Zn and Zr contents is illustrated in Figure 12. It is clearly observed that the saturation magnetization of the system increases with increasing x content up to x = 0.3, and then decreases. The initial increase is due to the increase of the resultant sublattice magnetic moment on the basis of Neel's sublattice model [16]. The theoretical magnetic moment (μth) is given by:

$$\mu_{th} = |M| = |M_B| - |M_A| \quad (6)$$

This depends on the substitution of magnetic ion at both A and B sites (cation distribution). Thus, the general formula of the theoretical magnetic moment is given by:

$$\mu th = [1.73(1-x) + 5(2x+2y-2t)]\ \mu B \quad \text{, where } t = 0.2y \quad (7)$$

where μB is Bohr magneton.

Using the saturation magnetization obtained from the hysteresis loop, the values of the experimental magnetic moment has been calculated using the following formula [17]:

$$\mu_{ex} = \frac{M\ W * M_S}{\mu_B * N} \quad (8)$$

where M_s is the saturation magnetization in (emu/cc) which is given by: $M_s = (1-p)*\sigma_s*d$

The experimental magnetic moment (μ_{ex}) decreases above x = 0.3 indicating the possibility of non collinear spin canting effect in the systems [18-21]. The presence of canting spin gives a rise to the Yafet-Kittel angle (α) which determines the strength of A-B and B-B exchange interactions. The Yafet-Kittel angle has been calculated at room temperature using the following formula [22]:

$$\mu_{ex} = M_B \cos \alpha_{Y\text{-}K} - M_A \quad (9)$$

It is clear that the values of Y-K angle, as reported in Table (6), increase with increasing Zn and Zr contents. The variation of μ_{ex} and μ_{th} as a function of Zn and Zr contents measured at room temperature are shown in Figure 13.

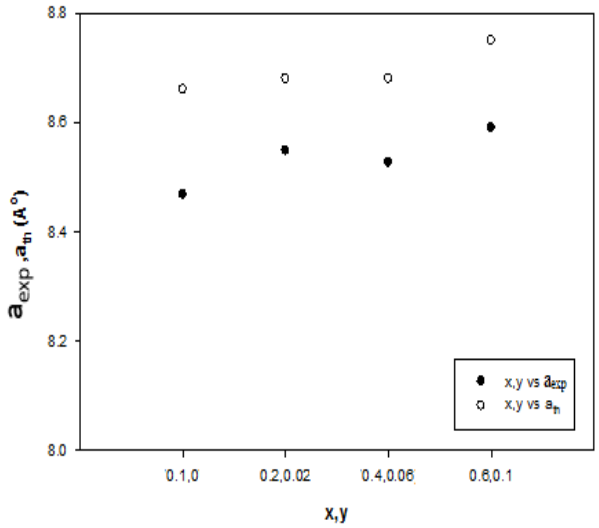

Fig. (6): The experimental and theoretical lattice parameter for (s) samples

Table (2): Variation of (u) and (δ) for (s) systems

x	y	u (Å)	δ (Å)
		Stoichiometric	
0.1	0.00	0.386	0.011
0.2	0.02	0.387	0.012
0.4	0.06	0.388	0.013
0.6	0.10	0.389	0.014

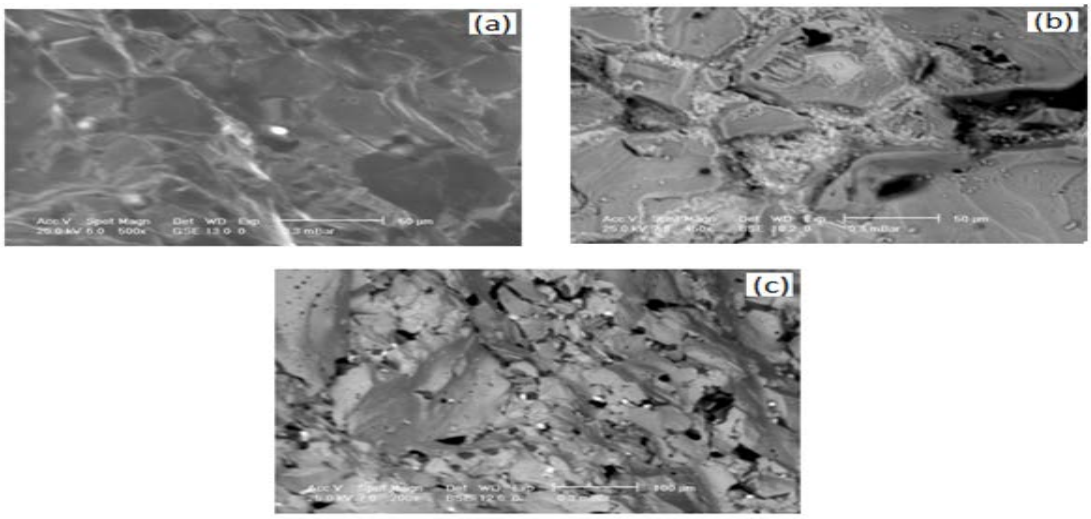

Fig. (7): The SEM micrograph for (s) Ferrite (a)x=0.1, y=0 (b)x=0.2,y=0.02 (c)x=0.4,y=0.06

Table (3): Evolution of grain size for (s) systems

(s)	Grain size (µm)
x = 0.1, y = 0.0	39.79
x = 0.2, y = 0.02	70.47
x = 0.4, y = 0.06	14.05

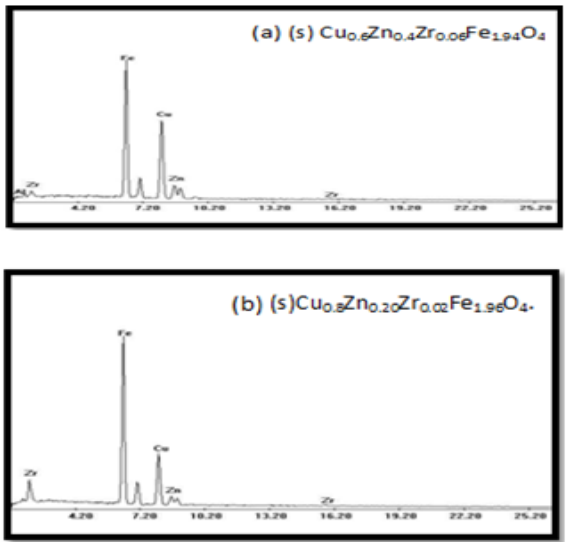

Fig. (8): The EDS spectrum (a) (s)$Cu_{0.6}Zn_{0.4}Zr_{0.06}Fe_{1.94}O_4$ and (b) (s)$Cu_{0.8}Zn_{0.22}Zr_{0.02}Fe_{1.96}O_4$

Table (4): Chemical composition as obtained by EDS analysis

	x	y	Atomic ratio % for elements			
			Cu	Zn	Zr	Fe
(s)	0.1	0.00	35.20	1.80	4.46	38.71
(s)	0.2	0.02	30.38	6.57	5.03	58.01
(s)	0.4	0.06	42.92	9.39	3.64	42.94

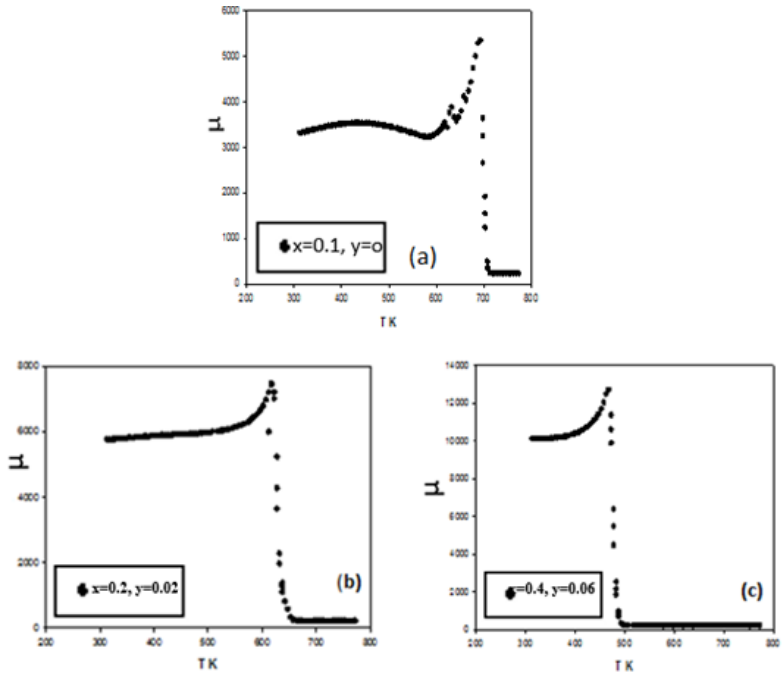

Fig. (9): The variation of initial permeability μi with temperature for (s) sample

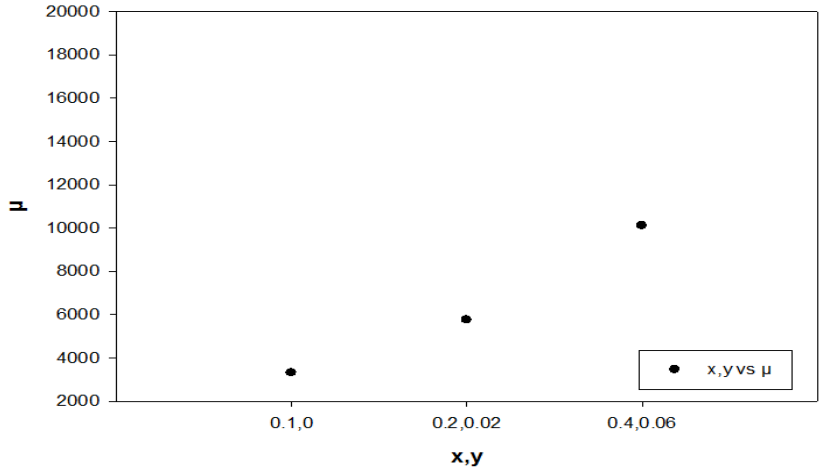

Fig. (10): The variation of permeability at room temperature with increasing x and y content for (s) sample

Table (5): Curie temperature (Tc) and the rate of change of μi

X	y y	T_c (K) Stoichiometric	Slope
0.1	0.00	708	324.1
0.2	0.02	653	286.7
0.4	0.06	488	667.7

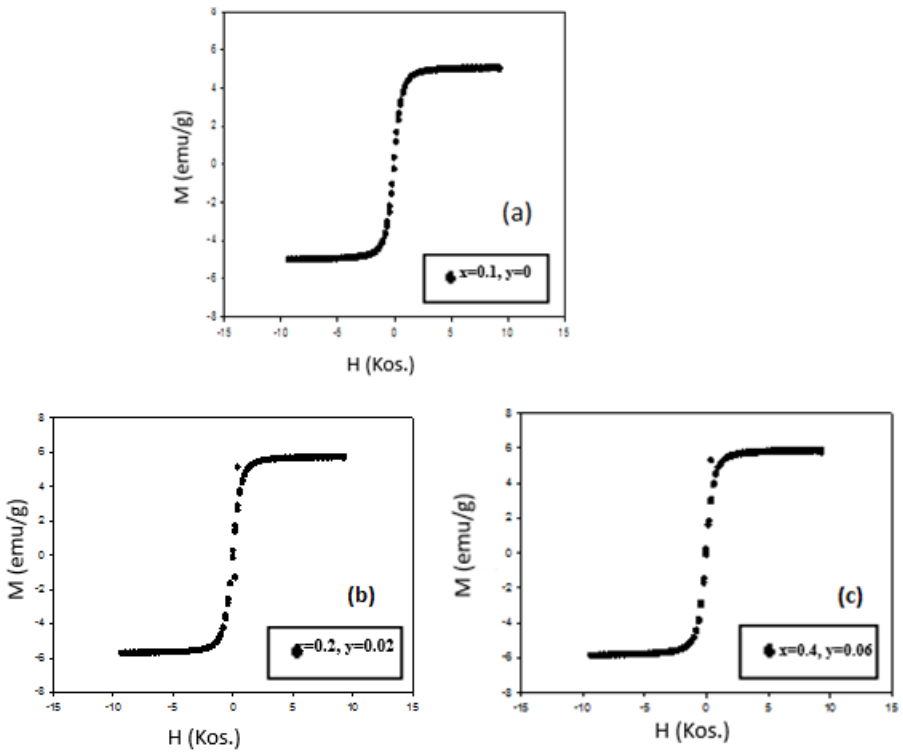

Fig. (11): The hysteresis loop for (s) sample

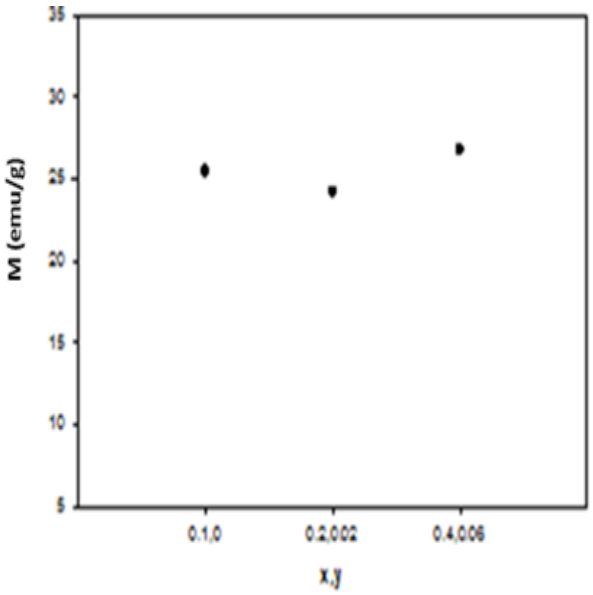

Fig. (12): The variation of saturation magnetization (M_s) with Zn and Zr content for (s) sample

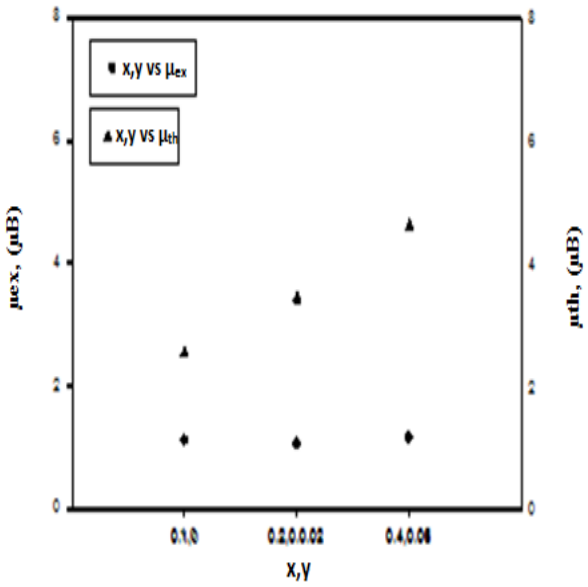

Fig. (13): The variation of μex and μth with x and y content for (s) sample

Table (6): Variation of α value with x and y contents

x	y	α
	Stoichiometric	
0.1	0.00	37.0
0.2	0.02	48.8
0.4	0.06	63.2

Conclusion

X-ray diffraction patterns confirm the formation of a single spinel cubic (fcc) phase for all compositions. Zn ions enhance the grain growth process to a certain limit whereas Zr retards the sintering process and grain growth. The system has a very high rate of change of permeability with temperature specially the composition with x = 0.4, making it a very promising candidate for temperature controller devices. The systems exhibit a typical magnetic hysteresis of a soft magnetic material, indicating that the obtained materials are magnetically ordered. Both saturation magnetization and experimental magnetic moment (μ_{ex}) are nearly constant.

References

1- Sattar, A.A., El-Sayed, H.M., Agami, W.R. and Ghani, A.A. Magnetic Properties and Electrical Resistivity of Zr4+ Substituted Li-Zn Ferrite. American Journal of Applied Sciences, 4 (2), 89-93, (2007)

2- H. E. Hassan, T. Sharshar, M. M. Hessien, O. M. Hemeda, Effect of γ-rays irradiation on Mn–Ni ferrites: structure, magnetic properties and positron annihilation studies. Nuclear Instruments and Methods in Physics Research Section B, 304 72-79(2013).

3- P. K. Chougule, S. S. Kumbhar, Y. D. Kolekar, C. H. Bhosale, Enhancement in Curie temperature of nickel substituted Co–Mn ferrite. Journal of Magnetism and Magnetic Materials, 372 181-186(2014).

4- K. Murakami, The characteristics of ferrite cores with low Curie temperature and their application IEEE Trans. Mag., MAG-I 96(1965).
5- D.I. Tchernev and T.E. Collier, Digital magnetic temperature transducer IEEE Trans. Mag., MAG-7450 (1971).
6- K. Seki, J. Shida and K. Murakami, IEEE Trans. Mag., MAG. 14 A new temperature telemeter with temperature-sensitive magnetic cores .14 -969(1978).
7- C. Tanasoiu, I. Nicolae, P. Nicolau and H. Niculescu, Ultrathermostat electronic components, Romanian Patent No. 76635 (1981).
8- C. Tanasoiu, I. Nicolae, P. Nicolau, H. Niculescu and C. Mihaiache, A new type of thermostat of high stability using a magnetic temperature transducer , J. Phys. E: Sci. Instr., 18 -50(1985).
9- B. D. Cullity, "Elements of X-ray Diffraction", Addison-Wesley, Reading, MA, 514(1959).
10- S.A. Mazen, M.H. Abdallah, R.I. Nakhla, H.M. Zaki, X-ray analysis and I.R. absorption spectra of Li-Ge ferrite. Mater. Chem. And physics 34 -35(1993).
11- Das, A.R., V.S. Ananthan and D.C. Khan, Lattice parameter variation and magnetization studies on titanium -, zirconium and tin substituted nickel -4189(1985). J. Appl. Phys. 57
12- A. Globus, P. Duplex, Effective Anisotropy in Polycrystalline Materials. Separation of Components ,J. Appl. Phys. 39 -727(1968).
13- A.G. Arias, F. Calderon, Physica Status Solidi Effect of Some Additives on Nickel-Zinc Ferrite Losses (a) 77 - K185(1983).
14- S. Ramesh, B. Dhanalakshmi. B. C. Sekhar, P.S.V. Subba Rao, B. P. Rao, Effect of Mn/Co substitutions on the resistivity and dielectric properties of nickel–zinc ferrites. Ceramics International Journal 42 (8) 9591–9598(2016).
15- A. Grusková, J. Sláma, M. Ušáková, M. Šoka, R. Dosoudil and J. Degmová, Study of Magnetic and Structural Properties of Non-Stoichiometric NiZn Ferrites Prepared by Wet Method 14th Czech and Slovak Conference on Magnetism, Košice, Slovakia, July 6–9, 2010. ACTA PHYSICA POLONICA A 118 -780(2010)
16- L. Neel, Ann. Phys. 3 -137(1948).
17- J. Smit, Magnetic Properties of Materials, Mcgraw Hill Book Co., p. 89(1971).
18- Y. Yafet, C. Kittel, Antiferromagnetic Arrangements in Ferrites .Phys. Rev. 87 -290(1952).
19- S. Geller, Comments on "Molecular-Field Theory for Randomly Substituted Ferrimagnetic Garnet Systems" by I. Nowik Phys. Rev. 181 -980(1969).
20- C.E. Patton, Y. Liu, Localised canting models for substituted magnetic oxides . J. Phys. C: Solid State Phys. 16 -5995(1983).
21- A. Globus, H. Pascard, V. Cagan, DISTANCE BETWEEN MAGNETIC IONS AND FUNDAMENTAL PROPERTIES IN FERRITES JOURNAL DE PHYSIQUE (Paris) 38 C1–C168(1977).
22- O. M. Hemeda, A. Tawfik, D. M. Hemeda, A. M. Elsheekh, Preparation and electrical properties of Ni–Cu–Zn system doped with the magnesium oxide International Journal of Modern Physics B. 28, 1450157(2014).